Atmos. Chem. Phys., 26, 13645–13660, 2026
https://doi.org/10.5194/acp-26-13645-2026

Atmospheric Chemistry and Physics
Open Access
EGU

Research article

Molecular-level characterization of urban aerosol analogues in controlled atmospheric simulations

Elie Al Marj[1], Ambre Delater[1], Aline Gratien[1], Marie Line Torrijos[1], Juan Camilo Macias Rodriguez[1], Mathieu Cazaunau[2], Edouard Pangui[2], Antonin Bergé[2], Cécile Gaimoz[2], Thomas Bertin[2], Emmanuelle Mebold[2], Bénédicte Picquet-Varrault[2], Jean-François Doussin[2], Clément Buissot[3], Sophie Lanone[3], and Patrice Coll[1]

[1]Université Paris Cité and Univ Paris Est Creteil, CNRS, LISA, 75013 Paris, France
[2]Univ Paris Est Creteil and Université Paris Cité, CNRS, LISA, 94010 Créteil, France
[3]Univ Paris Est Creteil, INSERM, IMRB, 94010 Créteil, France

Correspondence: Patrice Coll (pcoll@lisa.ipsl.fr)

Received: 28 March 2026 – Discussion started: 12 May 2026
Revised: 26 August 2026 – Accepted: 8 September 2026 – Published: 29 September 2026

Abstract. Urban air pollution consists of complex mixtures of gases and particulate matter. Understanding the molecular-level composition of these mixtures is essential for interpreting biological responses, but such characterization is difficult under ambient conditions. This study presents the chemical characterization of two controlled atmospheric scenarios generated in the CESAM smog chamber and transferred to the PolluRisk exposure isolator.

The standard urban scenario consisted of selected anthropogenic and biogenic volatile organic compounds (VOCs) with primary ammonium sulphate seed particles. The biomass burning enhanced scenario included the same precursors and seed particles, with additional wood-pellet combustion emissions. Solar simulator was continuously turned on throughout the experimental periods and no day/night or dark-aging cycle was applied. Mean PM_1 concentrations in the exposed isolator were $15 \pm 7\,\mu g\,m^{-3}$ for the standard urban scenario and $63 \pm 24\,\mu g\,m^{-3}$ for the biomass burning scenario. Organic aerosol represented approximately 17 % and 40 % of PM_1, respectively. Proton-transfer-reaction time-of-flight mass spectrometry (PTR-TOF-MS) identified 23 VOCs, with oxygenated compounds accounting for 74 %–77 %. Ultrahigh-performance liquid chromatography electrospray ionization ion mobility quadrupole time-of-flight mass spectrometry (UPLC/ESI-IMS-QTOFMS) revealed 32 distinct particle-phase compounds. The biomass burning scenario showed features compatible with combustion-related and oxidation-related products, including source-specific tracers such as a levoglucosan isomer, nitrophenolic compounds (e.g., 3-methyl-4-nitrocatechol, nitroguaiacol), and oxidized aromatics. Estimated volatility classes covered the semi-volatile, low-volatility, and extremely low-volatility organic compound ranges ($C^* < 300\,\mu g\,m^{-3}$), indicating substantial functionalization and partitioning. The two simulated scenarios showed distinct compositions under the controlled operating conditions. These measurements provide a chemical framework for separate biological exposure experiments. This framework is intended to support mechanistic exposure-health studies, to be reported in a companion manuscript. However, the experiments were not designed to reproduce the full chemical composition of ambient urban air, determine an equivalent atmospheric age, or quantify the relative contributions of primary and secondary organic aerosol.

Published by Copernicus Publications on behalf of the European Geosciences Union.

1 Introduction

Air pollution poses serious health risks worldwide, leading to millions of premature deaths each year (Slovic and Ribeiro, 2018). Without effective interventions, it is expected to become the major cause of early mortality by 2050 (Von Schneidemesser et al., 2015). Despite air quality measures by organizations like the World Health Organization (WHO), the rapid growth of cities and populations makes pollution issues in megacities even more challenging (Baudic et al., 2016; Salameh et al., 2019). Pollution mitigation policies have been effective in reducing exposure to primary pollutants (SO_2, NO_x). However, they remain insufficient in reducing pollution due to secondary pollutants such as ozone and secondary aerosol. This underscores the need for a detailed understanding of the complex atmospheric chemical processes that are responsible of the formation and transformation of secondary pollutants.

Understanding urban air pollution complexity requires a detailed knowledge of the composition of particulate matter, especially at the molecular level. The molecular composition of PM_1 particles could play key roles in toxicological responses, but these aspects remain poorly understood. A major obstacle in atmospheric research is the variability of ambient conditions, which complicate molecular characterization and limit the consistency of exposure studies (Finlayson-Pitts and Pitts, 2000; Seinfeld and Pandis, 2012). Atmospheric simulation chambers offer a complementary approach by allowing researchers to isolate specific emission sources and conduct detailed chemical analyses under reproducible conditions (Doussin et al., 2023).

Few studies have combined controlled atmospheric simulation with detailed molecular characterization specifically designed for biological exposure assessment. Furthermore, the limited number of studies that have coupled atmospheric chambers with biological exposure have generally relied on organic aerosol concentrations substantially exceeding ambient levels (e.g., Krug et al., 2018, generated a PM-focused surrogate atmosphere reaching 976 µg m^{-3}). The target PM_1 concentrations in the present study were selected to overlap with concentration ranges observed in the Paris region, whereas the molecular composition and temporal variability of the generated mixtures cannot be assumed to reproduce ambient urban air in full. This chemical characterization is designed to define exposure conditions for biological models, not to serve as a comprehensive ambient urban air replica. The first scenario includes selected anthropogenic and biogenic VOCs with ammonium sulphate seed aerosol. The second scenario involves the same mixture in addition to emissions from wood-pellet combustion. We compare their global composition, gas-phase products, particle-phase molecular features, and estimated volatility distributions. These scenarios are intended as controlled exposure atmospheres and are not presented as complete reproductions of ambient urban air.

This paper reports the chemical characterization of PM_1 and its organic molecular composition in the two controlled cases. We combine online measurements of particle, trace-gas, and VOC concentrations with offline UPLC/ESI-IMS-QTOFMS analysis of particle-phase extracts. The study identifies source-related and oxidation-related molecular features and estimates their volatility classes. These measurements define the chemical conditions for separate exposure experiments. Thus, the biological outcomes are outside the scope of the present paper. The associated biological and toxicological outcomes observed in murine exposure models will be reported in a companion paper currently in preparation.

2 Materials and methods

2.1 Pollurisk platform

The PolluRisk platform was developed at the Interuniversity Laboratory of Atmospheric Systems (LISA UMR CNRS 7583) in collaboration with the Mondor Institute for Biomedical Research (IMRB UMR U955 INSERM) located in Créteil, France. The fundamental concept of the PolluRisk platform (Fig. 1) is to simulate urban atmospheric pollution scenarios in a controlled environment, allowing researchers to expose biological models (e.g., mice) and study the resulting health effects. This platform has been previously described in several studies (Belgacemi et al., 2023; Blayac et al., 2024; Coll et al., 2018; Georgopoulou et al., 2024; Guilloteau et al., 2022).

Central to the platform is the CESAM atmospheric simulation chamber (http://cesam.cnrs.fr, last access: 21 September 2026), a 4.2 m^3 stainless steel reactor designed to reproduce multiphasic oxidation processes. A detailed CESAM description is provided by Wang et al. (2011). The chamber achieves controlled precursor concentrations, with mixing times of approximately one minute ensuring gaseous compound homogeneity. An artificial irradiation system powered by three 6.5 kW high-pressure Xenon arc lamps (IREM, EX170GM3) facilitates atmospheric photochemistry, achieving a JNO_2 value of 8.3×10^{-3} s^{-1}. Pyrex® filters reduce ultraviolet radiation intensity, especially below 300 nm, reproducing tropospheric solar radiation. The chamber maintains evacuable conditions (reaching 10^{-7} atm) with pumping systems capable of removing adsorbed compounds. Relative humidity (RH) was maintained at 30 %–50 % on average to promote condensational growth of organic material onto pre-formed ammonium sulphate seed particles, while avoiding water condensation interference with organic aerosol formation. RH was maintained constant across both scenarios to ensure experimental comparability. We acknowledge that real biomass burning episodes typically occur at higher RH (60 %–80 %), which would enhance gas-particle partitioning (Sect. 4.3).

To study the induced health effects, the generated atmosphere is continuously transferred through a 3/8 in. cop-

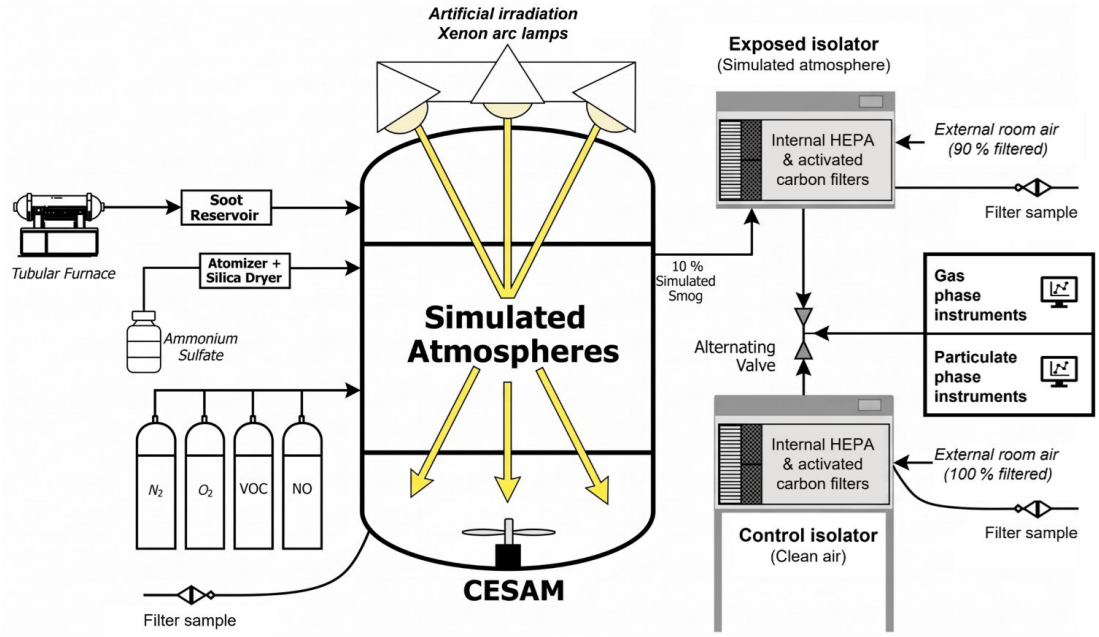

Figure 1. Schematic diagram of the PolluRisk experimental platform, illustrating the CESAM atmospheric simulation chamber equipped with a Xenon lamp irradiation system, two isolators for mice exposure (the exposure isolator receiving 90 % filtered laboratory air using HEPA and activated carbon filters and 10 % simulated air in CESAM, and the reference isolator receiving 100 % of filtered room air), and the multi-instrument analytical set for pollutant characterization.

per line inside an isolator (I-Box+ Erlab, Noroit®), via an overpressure of 7 mbar applied in the smog chamber. This overpressure ensures continuous flow to the exposure isolator while preventing atmospheric contamination. The isolator houses experimental mice in individual cages (up to 19 cages) with controlled ventilation. The exposure isolator also receives filtered laboratory air (HEPA- and activated carbon-filtered room air, removing particles > 0.3 µm and gaseous compounds, respectively) with 90 % filtered room air and 10 % simulated smog atmospheres. This results in an atmosphere dilution ratio of 1 : 10 between CESAM and the exposure isolator. In addition to the exposure isolator, another isolator receives only filtered laboratory air and serves to house the reference mice group. Using one-way valves, both isolators are connected to a manifold system. The latter is connected to analytical instruments for the analysis of gas and particulate pollutants. Measurements of particles and gases were performed via a manifold system alternating between the exposure isolator (4 h) and the reference one (1 h), across 7 consecutive days of continuous monitoring (24 h d^{-1}). Irradiation was maintained continuously throughout the 7 d experiments without day/night cycling. While this ensures stable aerosol generation for chronic biological exposure, it differs from ambient photochemical cycling between OH-dominated daytime and NO_3-dominated night-time chemistry.

All pollutant concentrations and chemical characterisation results presented in this manuscript refer to measurements performed in the exposure isolator, which constitutes the actual biological exposure environment. CESAM serves exclusively as the aerosol generation and photochemical aging system. This paper presents the results of the measurements in the exposure isolator. The resulting health impacts will be described in a subsequent paper.

2.2 Particulate and gaseous precursors

Following the PolluRisk platform methodology (Coll et al., 2018), we used a VOC mixture with concentrations determined by box modelling to achieve target urban pollution levels after photochemical processing in CESAM. Among the primary pollution sources affecting moderately polluted cities, road traffic represents a major VOC contributor. In Paris, for instance, this source accounts for approximately 25 % of annual VOC emissions, with toluene and m-xylene as major traffic-related aromatics, contributing to nearly 20 % of this fraction, while long-chain alkanes (such as tridecane) result from diesel emissions (Gaimoz et al., 2011; Languille et al., 2020). Biogenic emissions such as α-pinene and isoprene can dominate during warmer periods, contributing up to 30 % of oxygenated compounds (Ait-Helal et al., 2014; Baudic et al., 2016; Gaimoz et al., 2011). To replicate these urban environments, we selected representative anthropogenic VOCs including aromatic hydrocarbons (toluene (P. Normapur®, PROLABO, puriss grade), m-xylene (Touzart & Matignon, 99 % purity)) and an aliphatic hydrocarbon (tride-

cane (Sigma-Aldrich, CAS 629-50-5, 99 % purity)), alongside biogenic VOCs (α-pinene (Sigma-Aldrich, CAS 80-56-8, $\geq$ 97.5 % purity), methylglyoxal (Sigma-Aldrich, CAS 78-98-8)) due to their atmospheric reactivity and SOA formation potential.

Ammonium sulphate particles (Sigma-Aldrich, CAS 7783-20-2, $\geq$ 99.9 % purity) were generated to simulate inorganic seed aerosols and to allow the condensation of secondary organic products resulting from the oxidation of VOCs. For biomass burning simulation, commercially available pellets compliant with EN ISO 17225-2 standards (70 % beech, 30 % conifers, ash $<$ 0.6 %, RH $<$ 8 %) were used as the biomass source (0.5–1.0 g per combustion cycle).

2.3 Experimental simulation of atmospheric scenarios

This study simulated two atmospheric scenarios for biological exposure assessment. Target PM_1 and NO_2 concentrations were selected with reference to ranges reported for the Paris region (AirParif, 2019; Petit et al., 2014; von der Weiden-Reinmüller et al., 2014). These comparisons concern selected concentration indicators only. They do not imply that either scenario reproduces the full chemical composition, temporal variability, or atmospheric processing of ambient urban air.

To achieve these representative urban conditions, all particulate and gaseous precursors were continuously injected into the CESAM smog chamber, previously filled with synthetic air (nitrogen N_2 and oxygen O_2) in 80 : 20 proportions. Tanks of pressurized liquid nitrogen (Messer, $\geq$ 99.9 % purity, H_2O content $<$ 5 ppm) and oxygen (Air Liquide, AlphagazTM Class 1, $\geq$ 99.9 % purity) were used to generate the N_2 and O_2. A 10^{-2} M ammonium sulphate solution was nebulized using a commercial atomizer (TSI Model 3075), followed by silica-gel dehumidification (TSI Model 3062). The biomass burning emissions were generated using a tubular furnace (CarboliteTM CTF Wire-Wound Tube Furnace) operated at 400 °C under controlled airflow conditions (3 L min^{-1} synthetic air). Emissions were continuously transferred to an auxiliary chamber at 1 L min^{-1}, then introduced into CESAM for atmospheric aging (Fig. 1). Combustion occurred twice daily while refilling the furnace every 10 to 12 h, ensuring steady carbonaceous particle supply. A homemade VOC mixture (methylglyoxal (13 ppm), toluene (25 ppm), m-xylene (22 ppm), tridecane (33 ppm), and α-pinene (8 ppm)) was continuously injected into the smog chamber at a constant flowrate of 0.05 L min^{-1} following (Doussin et al., 2023) methodology for chamber protocols. After 20–30 h, nitrogen monoxide (NO, Air Liquide, 99.5 % purity) was introduced at 0.5 L min^{-1}. Nitrogen monoxide was used to establish the NO-NO_2-O_3 photostationary cycle, promoting OH radical formation through NO_2 photolysis and enhancing VOC oxidation under high NO_x conditions representative of urban photochemical regimes. Irradiation began 11 h before exposure initiation to reach a steady state and replicate tropospheric photochemistry. Irradiation was maintained continuously throughout the entire experimental period to ensure stable photochemical conditions.

This study simulated atmospheric scenarios characteristic of moderately polluted urban environments, focusing on two distinct cases representing different emission source contributions:

1. The standard urban scenario simulated baseline urban conditions. It included the selected anthropogenic and biogenic VOC mixture (methylglyoxal, toluene, m-xylene, tridecane, α-pinene) together with ammonium sulphate seed particles. It was designed to examine secondary organic aerosol formation from the injected VOC mixture and did not include primary carbonaceous or traffic-emitted particulate matter.

2. The biomass burning enhanced scenario involved the same VOC mixture and ammonium sulphate seed particles, with the continuous addition of wood-pellet combustion emissions. These emissions provided primary carbonaceous particles and additional gas-phase compounds. The resulting difference between scenarios therefore combines primary particulate input, additional gaseous emissions, and their subsequent atmospheric processing.

2.4 Analytical Instrumentation

A comprehensive analytical suite enabled detailed characterization of both gas-phase and aerosol-phase components, including concentration measurements, chemical composition analysis, and molecular-level identification.

2.4.1 Global characterization of particle and gas phases

Aerosol size distribution (19.5–881.7 nm) was measured using a scanning mobility particle sizer (SMPS) consisting of a differential mobility analyser (DMA, TSI 3080) and a condensation particle counter (CPC, TSI 3772) with 2 min resolution. Non-refractory submicron particle components (NR-PM_1, aerodynamic diameter between 40 nm and 1 µm) including sulphates, nitrates, ammonium, organics, and chlorides were analysed using a time-of-flight aerosol chemical speciation monitor (TOF-ACSM, Aerodyne Research Inc.). This instrument operated with a 6 min data acquisition and a collection efficiency (CE) of 0.5 for organics (Middlebrook et al., 2012). Particles were vaporized at 600 °C and ionized by 70 eV electron impact before mass spectrometric separation and detection. Particle mass concentrations were calculated from measured particle number size distribution, assuming particles sphericity and a calculated density following Salcedo et al. (2006).

Nitrogen oxides (NO_x), ozone (O_3), and carbon monoxide (CO) were monitored using Horiba® APNA 370®, APOA 370®, and ProCeas AP2e analysers. VOCs were measured

using proton transfer reaction-time-of-flight-mass spectrometry (PTR-TOF-MS, Kore Technology LTD, Series II) at 1 min resolution. The PTR-TOF-MS was operated using H_3O^+ ions with a drift tube pressure of 1.3 mbar, temperature of 60 °C, and voltage of 400 V (E/N approximately 145 Td). Data were acquired in the m/z range from 20 to 130. Individual VOC concentrations were quantified following established quantification protocols by (De Gouw and Warneke, 2007) and reported by (Michoud et al., 2017). Systematic calibration was conducted before each experiment using gas calibration units (Ionicon®) containing VOC standards.

To complement overall aerosol composition measurements and achieve detailed molecular characterization of organic components, offline filter-based analytical techniques were used.

2.4.2 High-resolution investigation of particle phase at the molecular level

Secondary organic aerosols were characterized at the molecular level using ultrahigh performance liquid chromatography electrospray ionization coupled to ion mobility time of flight mass spectrometry (UPLC/ESI-IMS-QTOFMS, Waters), as described by Pereira et al. (2026). Prior to analysis, filters were spiked with 5 µL of (1S)-(+)-camphor-10-sulfonic acid (Sigma Aldrich, 0.5 mg L^{-1}) as internal standard. Filter extraction used acetonitrile (ULC/MS-CC/SFC grade, Biosolve) with room temperature shaking (Mini Shaker, VWR, 1000 rpm, 30 min), followed by 0.2 µm filtration (VWR Syringe Filter, hydrophobic PTFE) and nitrogen stream evaporation (N-Evap 12 positions, Organomation). Samples were redissolved in 200 µL of 50/50 acetonitrile / ultrapure water mixture and stored at −18 °C until analysis. UPLC/ESI-IMS-QTOFMS analyses were performed using a Vion IMS-QTOF mass spectrometer (Waters) coupled to an Acquity UPLC system equipped with a BEH C18 column (1.7 µm, 2.1 × 100 mm). Analyses were performed in triplicate with 2 µL injection volume. Mobile phases consisted of ultrapure water (A) and acetonitrile (B), both acidified with 0.1 % formic acid, with a 45 min gradient at 0.4 mL min^{-1}. The electrospray source was operated in negative ionization mode (desolvation temperature 250 °C, m/z range 50–1000). Compound identification relied on two approaches: compounds matched against an existing database containing retention time, collision cross-section, and accurate mass for confirmed standards, and tentative identification based solely on accurate m/z matching for compounds without available standards.

To characterize volatility distribution, we applied the group contribution method developed by Donahue et al. (2011). We note that alternative volatility estimation methods (e.g., the parametrization of Li et al., 2016) may yield different $\log C$ estimates for the same compounds. Values reported here should therefore be considered indicative rather than absolute. This approach estimates saturation mass concentrations (C) (determined based on the web platform "UManSysProp") from calculated vapor pressures at 298 K based on molecular structure and functional group contributions. Compounds were classified into volatility categories: volatile organic compounds (VOCs, $C^* > 3 \times 106\,\mu g\,m^{-3}$), intermediate-volatility compounds (IVOC, $300 < C^* < 3 \times 10^6\,\mu g\,m^{-3}$), semi-volatile organic compounds (SVOCs, $0.3 < C^* < 300\,\mu g\,m^{-3}$), low-volatility organic compounds (LVOCs, $3 \times 10^{-4} < C^* < 0.3\,\mu g\,m^{-3}$), and extremely low-volatility organic compounds (ELVOCs, $C^* < 3 \times 10^{-4}\,\mu g\,m^{-3}$). This classification supports the assessment of gas-particle partitioning tendencies and secondary organic aerosol formation potential for both injected precursors and detected transformation products (Donahue et al., 2006, 2011).

2.5 Summary of the experiment

The complete experimental workflow (Fig. 2) illustrates the five main methodological steps: (1) simulation setup with VOC injection, seed aerosol generation, and optional biomass burning emissions; (2) atmospheric aging under controlled irradiation; (3) controlled exposure in isolators with alternating sampling protocols; (4) extensive sampling and analysis using online monitoring (PTR-TOF-MS, ACSM, SMPS), offline filter collection, and molecular characterization (UPLC/ESI-IMS-QTOFMS); and (5) data processing yielding chemical composition profiles, molecular markers, volatility distributions, and source-specific signatures for each exposure scenario.

3 Results

The experimental design generated distinct atmospheric scenarios over the 7 d periods in the exposure isolator (Fig. 3). The temporal profiles (exposure isolator) show controlled fluctuations associated with precursor photochemical processing and, for the biomass burning enhanced scenario, periodic combustion cycles. The biomass burning enhanced scenario generally led to higher concentrations than the standard urban one for the measured parameters throughout the entire exposure duration.

We characterized both scenarios in the exposure isolator through complementary analytical approaches, focusing on compositional differences. Hence, we based our analysis on two levels of investigation: PM and gas concentrations (Sect. 3.1), and the molecular composition of aerosols (Sect. 3.2). These analyses (exposure isolator) were then compared with regard to ambient air data and field studies results.

3.1 Global investigation of particle and gas phases

In the exposure isolator, PM_1 concentrations averaged $15 \pm 7\,\mu g\,m^{-3}$ for the standard urban scenario and

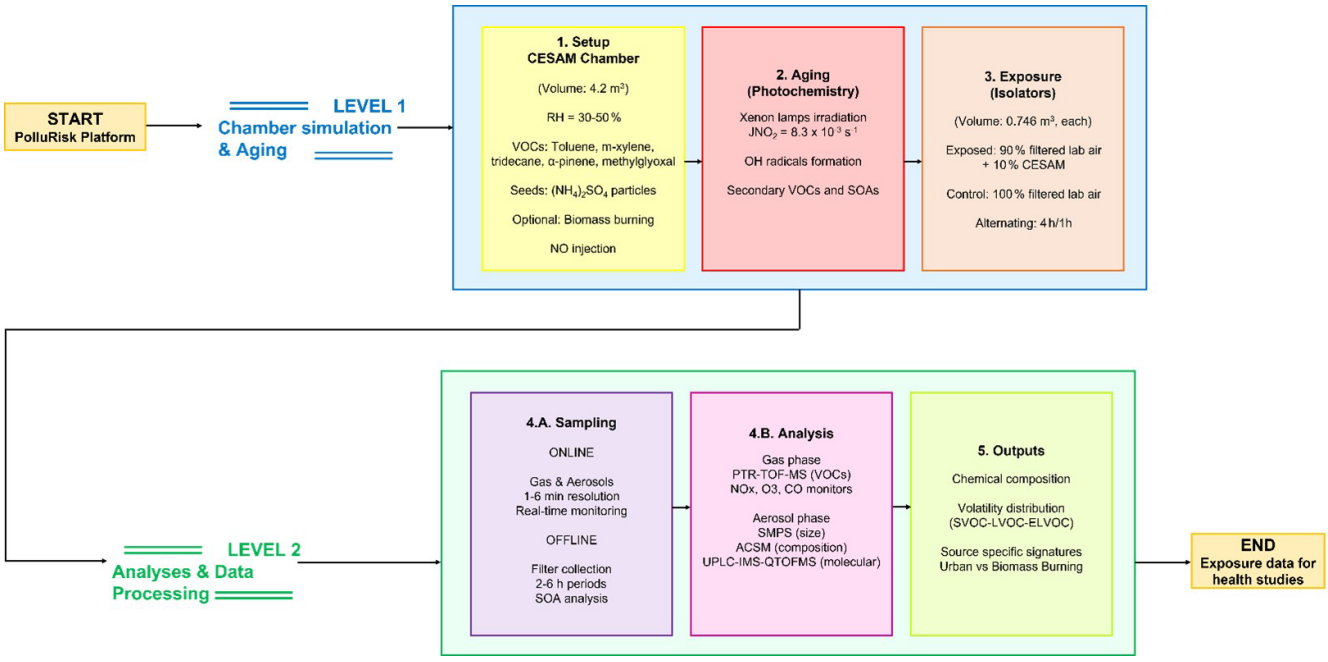

Figure 2. Complete experimental workflow. Two-sequence workflow: chamber simulation and aging processes, followed by analytical procedures and data processing. Colour coding: yellow = setup phase, red = photochemical aging, orange = exposure conditions, purple = sampling/analysis, green = final outputs. Flow direction: horizontal arrows indicate sequential progression, vertical arrow shows transition from chamber to analytical levels. END indicates completion of exposure protocol for health studies.

$63 \pm 24\,\mu g\,m^{-3}$ for the biomass burning enhanced scenario. Non-refractory PM_1 chemical composition revealed distinct exposure profiles between scenarios (Table 1). Standard urban simulation showed sulphate dominance (approximately 42 %), followed by ammonium (approximately 29 %) and organics (approximately 17 %). The biomass burning enhanced simulation showed that organics contributed approximately 40 % of PM_1 mass, driven by carbonaceous particles and their atmospheric aging under controlled irradiation. Nitrates accounted for approximately 20 %, reflecting secondary formation through NO_2 oxidation. The calculated aerosol densities were $1.77\,g\,cm^{-3}$ for the standard urban scenario and $1.59\,g\,cm^{-3}$ for the biomass burning enhanced scenario.

Average NO_2 concentrations reached 27 ± 10 ppb for the standard urban scenario and 39 ± 4 ppb for the biomass burning enhanced scenario. Carbon monoxide concentrations increased from 171 ± 63 ppb (standard urban) to 472 ± 92 ppb (biomass burning enhanced). Ozone concentrations averaged 4 ± 3 ppb (standard urban) and 9 ± 5 ppb (biomass burning enhanced).

PTR-TOF-MS allowed the identification and quantification of 23 distinct VOCs, including both primary emissions and secondary oxidation products. Complete compound list with m/z values, O : C ratios, volatility classifications, and calculated concentrations is provided in Table 2.

Figure 4 illustrates VOC classification by chemical families. Oxygenated compounds dominated both scenarios (74 % standard urban, 77 % biomass burning), with carboxylic acids predominant (31 % standard, 42 % biomass burning).

3.2 High-resolution investigation of particle phase at the molecular level

Building upon global composition measurements, molecular-level analysis of particle phase revealed the specific organic compounds driving compositional differences between scenarios. After thorough peak selection and analysis using Waters UNIFI software, we identified 32 distinct organic compounds. Of these, only 4 were detected in both scenarios, while the remaining 28 were exclusively identified in the biomass burning enhanced scenario. Compound identification was assigned to two confidence levels following Schymanski et al. (2014): level 1 for compounds confirmed with authentic standards and level 2 for tentative identifications based on accurate mass and fragmentation information. These compounds span multiple chemical families including nitrophenols, biogenic oxidation products, ring-opening products, anhydrosugars, and other oxidation products. The complete list, including retention times, m/z values, O : C ratios, and estimated volatility classes, is provided in Table 3.

Aromatic oxidation (toluene and m-xylene) produced both ring-retaining compounds including 2,3-dihydroxy-4-oxopentanoic acid (DHOPA), 4-nitrophenol, dimethylnitrophenol and 3-methyl-4-nitrocatechol, as well as ring-

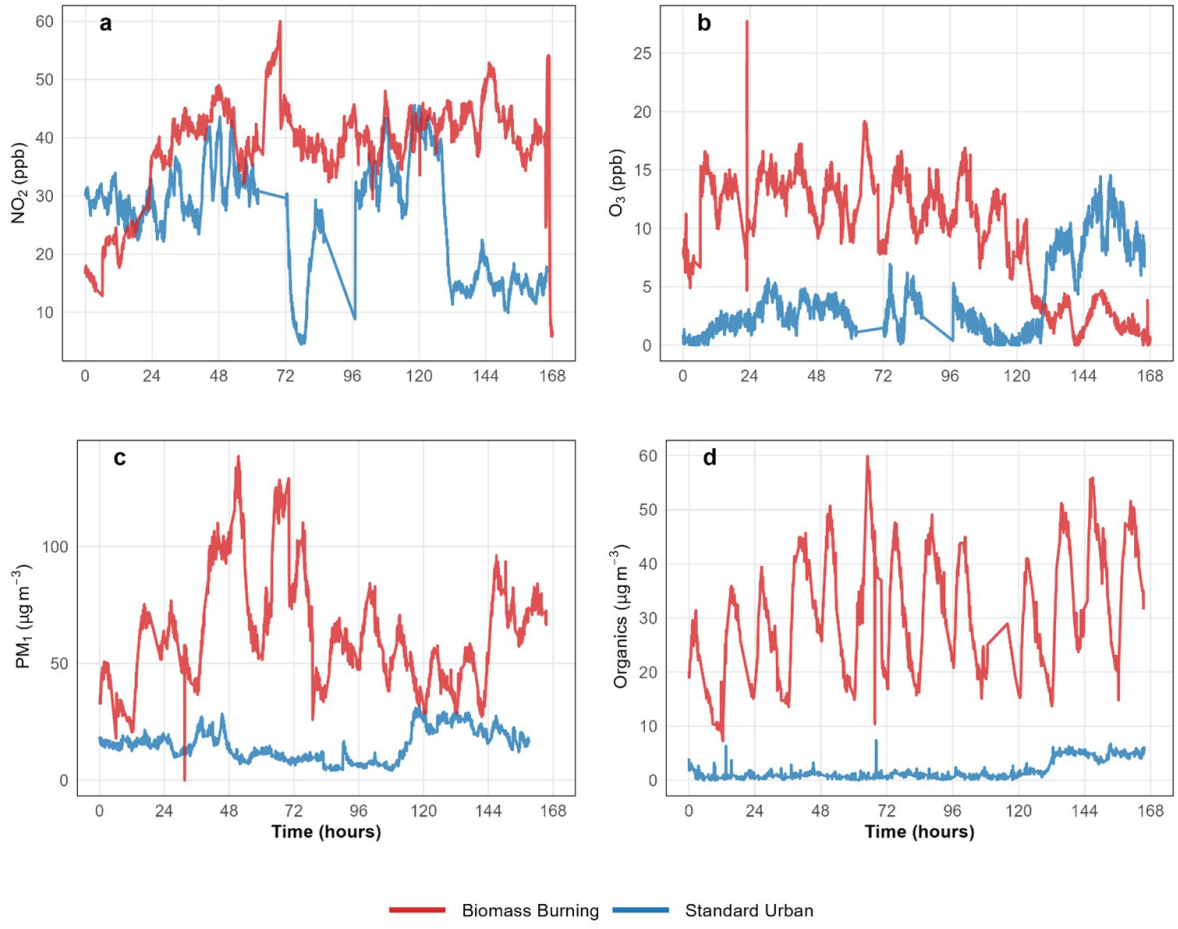

Figure 3. Temporal evolution of key pollutants during standard urban (blue) and biomass burning enhanced (red) exposure experiments: **(a)** NO_2, **(b)** O_3, **(c)** PM_1 concentrations, and **(d)** organic aerosol mass.

Table 1. Non-refractory PM_1 chemical composition measured during standard urban and biomass burning enhanced atmospheric simulations. Values represent means ± standard deviations calculated from temporal variations throughout the 7 d exposure periods.

Scenario	SO_4^{2-} ($\mu g\,m^{-3}$)	NH_4^+ ($\mu g\,m^{-3}$)	NO_3^- ($\mu g\,m^{-3}$)	Cl^- ($\mu g\,m^{-3}$)	Organics ($\mu g\,m^{-3}$)
Standard urban	3.6 ± 2.3	2.5 ± 1.4	1.3 ± 1.4	< LOD	1.7 ± 1.8
Biomass burning enhanced	21.4 ± 11.2	13.8 ± 7.0	12.5 ± 5.6	< LOD	31.1 ± 11.3

opening products such as succinic acid, demonstrating multiple oxidation pathways for aromatic precursors under controlled conditions. We identified biogenic oxidation products including pinic acid, cis-pinonic acid, norpinonic acid, and 3-methyl-1,2,3-butanetricarboxylic acid (MBTCA).

We detected several compounds derived from biogenic and anthropogenic precursor oxidation in both scenarios, though we were able to achieve more comprehensive detection in biomass burning enhanced conditions due to higher organic aerosol concentrations. 4,6-dinitro-o-cresol (from aromatic precursor oxidation under high NO_x), dimethyl-nitrophenol (from m-xylene oxidation), and cis-pinonic acid (from α-pinene ozonolysis and OH radical oxidation) were identified in both scenarios. The limited number of compounds detected in both scenarios may reflect analytical detection limits rather than the absence of those compounds, as standard urban organic aerosol concentrations ($1.7\,\mu g\,m^{-3}$) were substantially lower than biomass burning levels ($31.1\,\mu g\,m^{-3}$). We also identified primary biomass burning emission markers, including a levoglucosan isomer, using m/z matching without retention time confirmation. This annotation should therefore remain tentative.

Quantification was attempted for five representative SOA markers (2-nitrophenol, cis-pinonic acid, MBTCA, norpinic

Table 2. Identified PTR-TOF-MS peaks, their chemical classification, Log(C^*) (determined using "UManSysProp" web platform) and concentrations observed for the simulated atmospheres. Concentration values represent means ± standard deviations over the experimental period.

m/z	Potential identified species	Chemical classification	O : C	Log(C^*)	Urban scenario concentration (ppb)	Biomass burning scenario concentration (ppb)
31.011	Formaldehyde – CH_2O	Carbonyl (Aldehyde)	1.00	8.29	14 ± 7	14 ± 2
33.033	Methanol – CH_3OH	Alcohol	1.00	8.29	49 ± 31	51 ± 28
41.031	Propadiene – C_3H_4	Hydrocarbon (Alkene)	0.00	9.34	6 ± 2	12 ± 3
42.029	Acetonitrile – C_2H_3N	Nitrile	0.00	8.01	3 ± 1	2 ± 1
45.041	Acetaldehyde – C_2H_4O	Carbonyl (Aldehyde)	1.00	5.81	2 ± 1	9 ± 2
47.013	Formic acid – CH_2O_2	Carboxylic acid	2.00	6.09	14 ± 8	26 ± 6
55.059	1,3-butadiene – C_4H_6	Hydrocarbon (Alkene)	0.00	8.86	13 ± 6	18 ± 13
57.056	Acrolein – C_3H_4O	Carbonyl (Aldehyde)	0.33	7.49	1 ± 1	1 ± 1
59.035	Acetone – C_3H_6O	Carbonyl (Ketone)	0.33	7.49	7 ± 4	8 ± 2
61.034	Acetic acid – $C_2H_4O_2$	Carboxylic acid	1.00	5.81	22 ± 16	77 ± 37
62.016	Nitromethane – CH_3NO_2	Hydrocarbon (Nitro-compound)	2.00	4.29	10 ± 3	13 ± 2
62.992	Ethylene glycol – $C_2H_6O_2$	Alcohol	1.00	5.81	25 ± 6	18 ± 3
69.048	Furan – C_4H_4O	Furan	0.25	7.04	3 ± 1	3 ± 2
71.056	Methyl-vinyl ketone (MVK) – C_4H_6O	Carbonyl (Ketone)	0.25	7.04	3 ± 1	4 ± 2
73.038	Methylglyoxal – $C_3H_4O_2$ (*Precursor*)	Carbonyl (Aldehyde)	0.67	5.46	8 ± 4	7 ± 3
75.045	Glyoxylic acid – $C_2H_2O_3$	Carboxylic acid	1.50	3.63	30 ± 17	49 ± 22
83.086	2-methylfuran – C_5H_6O	Furan	0.20	6.59	10 ± 5	16 ± 9
85.013	Ethyl vinyl ketone (EVK) – C_5H_8O	Carbonyl (Ketone)	0.20	6.59	9 ± 4	21 ± 5
89.024	Butanoic acid – $C_4H_8O_2$	Carboxylic acid	0.50	5.06	25 ± 13	27 ± 18
93.036	Toluene – C_7H_8 (*Precursor*)	Hydrocarbon (Aromatic)	0.00	7.44	6 ± 8	8 ± 2
97.006	Furfural – $C_5H_4O_2$	Carbonyl (Aldehyde) and Furan	0.40	4.65	10 ± 4	16 ± 3
107.076	Xylene – C_8H_{10} (*Precursor*)	Hydrocarbon (Aromatic)	0.00	6.96	3 ± 3	3 ± 1
127.059	1,2,3-benzenetriol – $C_6H_6O_3$	Hydrocarbon (Aromatic)	0.50	2.21	10 ± 4	13 ± 4

acid, and pinic acid) using camphor-10-sulfonic acid as an internal standard, following calibration curves established for each compound (Sect. S4, Supplement). Atmospheric concentrations were calculated by referencing the mass identified on the filter to the specific surface area analysed and the total volume of air sampled. Sampled volumes ranged between 0.51 and 0.56 m^3 for the CESAM chamber and 2.76 and 2.95 m^3 for the exposure isolator. Reliable quantification in the exposure isolator was limited by the 1 : 10 dilution from CESAM combined with the comparatively low organic aerosol loading achieved in this campaign, particularly for the standard urban scenario (1.7 $\mu g\, m^{-3}$), which approached instrumental detection limits for individual compound quantification. A confirmed quantified concentration was obtained for cis-pinonic acid in CESAM under standard urban conditions ($255 \pm 23\, ng\, m^{-3}$). Comprehensive isolator-level quantification of these markers for both scenarios was not achieved in this campaign and is identified as a priority for future campaigns with higher organic loadings or increased sampling frequency (Sect. 4.3). Qualitative detection was possible for the 32 molecular features even when compound-specific quantification was not completed. However, identifications based only on m/z remain tentative and should not be interpreted as definitive structural assignments (Table 3).

The volatility analysis identified compounds distributed across semi-volatile, low-volatility, and extremely low-volatility organic compound ranges (SVOCs, LVOCs, ELVOCs; $C < 300\, \mu g\, m^{-3}$). These estimates are structure-based and indicative rather than direct measurements of volatility or mass partitioning. The oxygen-to-carbon (O : C) ratios and estimated saturation mass concentrations (C^*) provide qualitative information on possible gas–particle partitioning behaviour, but the figure does not provide mass-weighted contributions to total organic aerosol.

The distribution of estimated volatility classes is consistent with the presence of functionalized organic compounds after photochemical aging. It does not, however, establish the extent of atmospheric aging or quantify gas-to-particle transfer. In particular, Fig. 5 represents the molecular diversity of the identified compounds across volatility classes and does not give information on the relative mass contributions of individual species to total organic aerosol.

4 Discussion and perspectives

The following discussion interprets our Results findings at two analytical levels: (1) global particle and gas phase characterization (Sect. 4.1), and (2) molecular-level organic composition (Sect. 4.2).

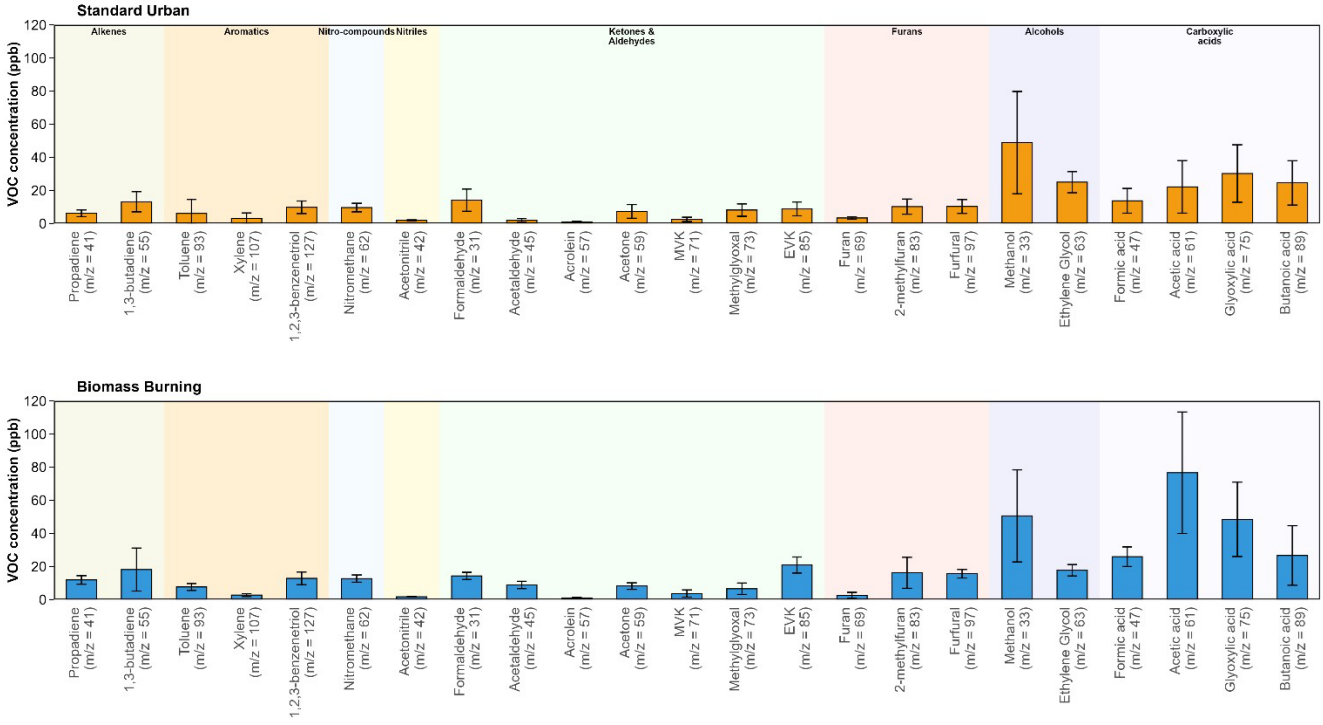

Figure 4. Average concentrations of volatile organic compounds (VOCs) identified in the exposure isolator by PTR-TOF-MS, organized by chemical families for standard urban scenario (orange bars) and biomass burning enhanced scenario (blue bars). Error bars represent ±1 standard deviation across the 7 d exposure period (MVK: methyl-vinyl ketone, EVK: ethyl vinyl ketone).

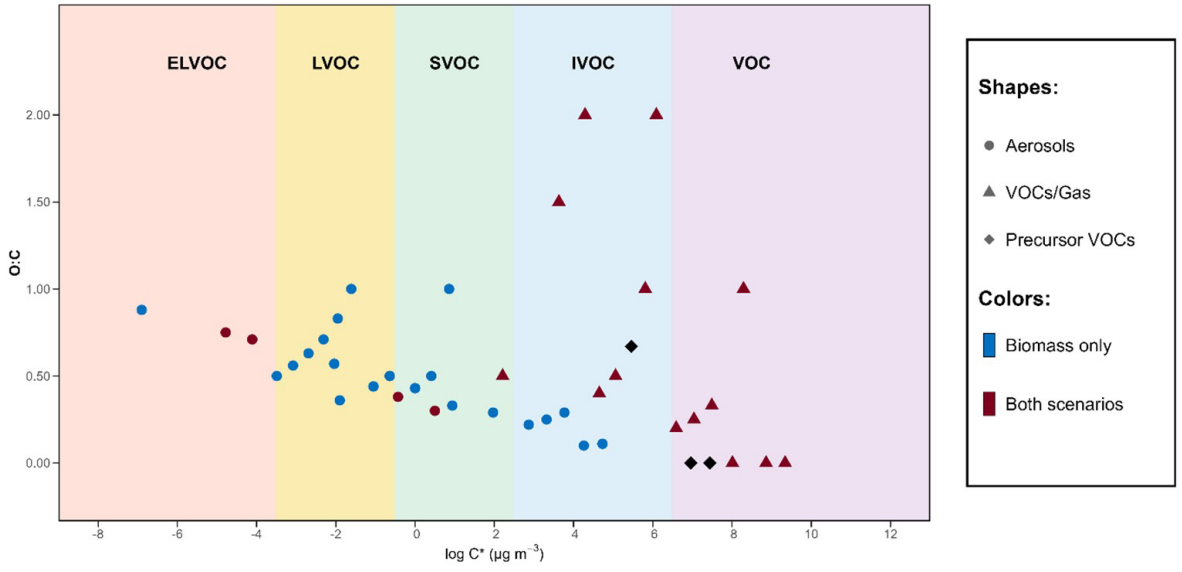

Figure 5. Molecular characterization of organic compounds identified in gas and aerosol phases, displayed as oxygen-to-carbon (O / C) ratios versus estimated volatilities (expressed as logarithm of saturation mass concentrations, C^*). Colour coding indicates compound volatilities, with blue symbols representing compounds detected in biomass burning enhanced scenario only and dark red symbols indicating compounds detected in both atmospheric scenarios. Diamond symbols (♦) indicate precursor VOCs initially injected into CESAM, circles (●) represent compounds detected by UPLC/ESI-IMS-QTOFMS, and triangles (▲) indicate compounds detected by PTR-TOF-MS.

Table 3. Summary of identified SOA products detected by UPLC/ESI-IMS-QTOFMS.

No.	Compound name	Molecular formula	Observed RT (min)	Observed m/z	O : C	Log(C^*)	Volatility	Scenario
1	Levoglucosan isomer	$C_6H_{10}O_5$	0.69	161.0457	0.83	−1.95	LVOC	BB
2	Dihydroxydimethoxyoxane-2-carboxylic acid	$C_8H_{14}O_7$	0.74	221.0663	0.88	−6.90	ELVOC	BB
3	3-Hydroxy-4,4-dimethylglutaric acid	$C_7H_{12}O_5$	2.85	176.8950	0.71	−2.31	LVOC	BB
4	3-methyl-1,2,3-butanetricarboxylic acid (MBTCA)	$C_8H_{12}O_6$	3.23	203.0558	0.75	−4.78	ELVOC	Both
5	3-acetylhexanedioic acid	$C_8H_{12}O_5$	3.43	187.0610	0.63	−2.69	LVOC	BB
6	Nitroguaiacol	$C_7H_7NO_4$	3.67	169.0135	0.57	−2.04	LVOC	BB
7	Terpenolic acid	$C_8H_{12}O_4$	3.72	171.0659	0.50	−0.64	LVOC	BB
8	5-propyldihydrofuran-2(3H)-one	$C_7H_{12}O_2$	3.93	127.0710	0.29	3.77	IVOC	BB
9	10-hydroxypinonic acid	$C_{10}H_{16}O_5$	4.57	215.0925	0.50	−3.49	LVOC	BB
10	Norpinic acid	$C_8H_{12}O_4$	4.89	171.0661	0.50	−0.64	LVOC	BB
11	2,3-dihydroxy-4-oxopentanoic acid (DHOPA)	$C_5H_8O_5$	5.35	148.9387	1.00	−1.61	LVOC	BB
12	Vanillylmandelic acid	$C_9H_{10}O_5$	5.36	197.0454	0.56	−3.08	LVOC	BB
13	5-butyldihydrofuran-2(3H)-one	$C_8H_{14}O_2$	6.20	141.0916	0.25	3.32	IVOC	BB
14	Pinic acid	$C_9H_{14}O_4$	6.20	185.0813	0.44	−1.05	LVOC	BB
15	5-nitrosalicylic acid	$C_7H_5NO_5$	6.45	182.0087	0.71	−4.11	ELVOC	BB
16	Norpinonic acid	$C_9H_{14}O_4$	7.04	185.0867	0.44	−1.05	LVOC	BB
17	3-pinalic acid	$C_9H_{13}O_3$	7.06	168.0867	0.33	0.94	SVOC	BB
18	4-nitrophenol	$C_6H_5NO_3$	8.55	138.0192	0.50	0.41	SVOC	BB
19	1-(2,2,3-trimethylcyclobutyl)ethan-1-one	$C_9H_{16}O$	9.10	139.1125	0.11	4.73	IVOC	BB
20	Cis-pinonic acid	$C_{10}H_{16}O_3$	9.10	183.1020	0.30	0.50	SVOC	Both
21	1R-(+)-Nopinone	$C_9H_{14}O$	9.14	183.1023	0.11	4.73	IVOC	BB
22	Sinapaldehyde	$C_{11}H_{12}O_4$	9.42	207.0661	0.36	−1.90	LVOC	BB
23	3-nitrotoluene	$C_7H_7NO_2$	10.51	182.0452	0.29	1.97	SVOC	BB
24	3-methyl-4-nitrocatechol	$C_7H_7NO_4$	11.23	168.0295	0.57	−2.04	LVOC	BB
25	2,6,6-trimethylnorpinan-3- one	$C_{10}H_{16}O$	12.15	151.1122	0.10	4.26	IVOC	BB
26	Benzyl nitrate	$C_7H_7NO_3$	13.01	152.0343	0.43	0.00	SVOC	BB
27	4-nitro-m/o-cresol	$C_7H_7NO_3$	13.09	152.0347	0.43	0.00	SVOC	BB
28	Succinic acid	$C_4H_6O_4$	13.15	117.9279	1.00	0.86	SVOC	BB
29	Norpinonaldehyde	$C_9H_{14}O_2$	13.76	153.0914	0.22	2.87	IVOC	BB
30	Dimethyl-nitrophenol	$C_8H_9NO_3$	15.64	166.0502	0.38	−0.43	SVOC	Both
31	4,6-dinitro-o-cresol	$C_7H_6N_2O_5$	16.10	197.0197	0.71	−4.11	ELVOC	Both
32	3-(2-propan-2-yl)pentanedioic acid	$C_8H_{14}O_4$	26.15	173.8707	0.50	−0.64	LVOC	BB

RT: retention time; C^*: saturation mass concentration at 298 K; Log(C^*) is determined using "UManSysProp" web platform; VOC: volatile organic compounds, IVOC: intermediate-volatility compound, SVOC: semi-volatile organic compound, LVOC: low-volatility organic compound, ELVOC: extremely low-volatility organic compound, BB: biomass burning scenario.

4.1 Global investigation of particle and gas phases

The temporal variations observed during the 7 d exposure periods (Fig. 3) document the ability to maintain distinct scenario-specific concentration ranges over extended periods. The day-by-day stability of the aerosol size distribution (Fig. S1a–b in the Supplement) supports the establishment of a quasi-steady state, consistent with continuous precursor injection and wall passivation.

The measured PM_1 concentrations in standard urban and biomass burning enhanced scenarios are, respectively, similar to those of summer background (10–20 µg m^{-3}) and winter pollution episodes (50–80 µg m^{-3}) in the Paris region (Petit et al., 2014; von der Weiden-Reinmüller et al., 2014). Organic aerosol concentrations show contrasting patterns between scenarios: standard urban levels (1.7 ± 1.8 µg m^{-3}) align with typical urban background measurements, while biomass burning enhanced concentrations (31.1 ± 11.3 µg m^{-3}) represent wintertime pollution episodes characteristic of residential wood burning periods in the Paris region (Languille et al., 2020; Petit et al., 2014; von der Weiden-Reinmüller et al., 2014).

However, VOC concentrations in both scenarios exceed typical ambient levels observed in Paris, where individual aromatic compounds rarely exceed 5–10 ppb (Gaimoz et al., 2011). The elevated VOC concentrations in our simulations (exceeding 20–50 ppb for several compounds) were defined to ensure sufficient secondary aerosol formation within the experimental timeframe, while maintaining realistic aerosol composition and mass concentrations for biological exposure studies.

Though, NO_2 concentrations are also typical of urban levels observed in the Paris region. These fall within ranges reported for moderate urban traffic conditions (20–40 ppb) and winter episodes (30–50 ppb), respectively (AirParif, 2019; von der Weiden-Reinmüller et al., 2014). Quantitatively, the concentration of CO highlights the contribution of biomass

combustion to exposure profiles to urban pollution during winter (Baudic et al., 2016). O_3 concentrations in both cases were below WHO guidelines. According to Sillman (1999), VOC-sensitive regimes are characterized by VOC/NO_x ratios < 4, while NO_x-sensitive regimes exhibit ratios > 15. In the urban photochemical regimes, high NO_x concentrations limit O_3 accumulation through ozone titration reactions ($NO + O_3 \rightarrow NO_2 + O_2$), hence reproducing the chemical behaviour typical of urban centres where ozone levels are suppressed despite high precursor concentrations (Seinfeld and Pandis, 2012).

Gas-phase characterization revealed scenario-specific VOC signals. Carboxylic acids accounted for 31 % of the reported signal in the standard urban mixture and 42 % in the biomass-burning-enhanced mixture. Oxygenated compounds accounted for 74 % and 77 %, respectively. The dominance of oxygenated compounds reflects photochemical aging of the precursor VOCs under controlled conditions, consistent with atmospheric transformation studies (Li et al., 2019; Montero et al., 2001). These observations are consistent with the oxidation of the injected precursors under the experimental conditions. The presence of glyoxylic acid (highest ratio of oxygen-to-carbon, O : C = 1.5) for instance, is indicative of highly oxidized products and has been attributed to toluene photooxidation products under high-NO_x conditions (Jang and Kamens, 2001).

The biomass burning enhanced scenario showed higher signals for several compounds, including formic acid ($m/z = 47$), acetic acid ($m/z = 61$), ethyl vinyl ketone (EVK, $m/z = 85$), and furfural ($m/z = 97$). For biogenic VOC transformations, the presence of MVK (methyl-vinyl ketone) was also evident. The differences are in line with the source specificities shown by Languille et al. (2020) in the Paris region.

Aerosol analysis showed a significant difference in chemical composition, with an organic fraction of approximately 17 % for the standard urban scenario against 40 % for the biomass burning scenario. The higher organic fraction in the biomass burning enhanced scenario is consistent with the added carbonaceous emissions and additional oxidation products, but these contributions were not quantitatively separated. The $[NO_3^-] / [SO_4^{2-}]$ ratio increased from 0.36 to 0.58. This observation indicates a compositional difference between both scenarios, reflecting secondary nitrate formation associated with biomass burning emissions (Bressi et al., 2013; Crippa et al., 2013; Petit et al., 2014; von der Weiden-Reinmüller et al., 2014).

The SMPS data (Fig. S1a–b) showed no detectable new particle formation below 30 nm in the presented time series and were consistent with growth on pre-existing particles under the experimental conditions (RH ∼ 40).

4.2 High-resolution investigation of particle phase at the molecular level

Molecular-level characterization identified a total of 32 distinct organic compounds, with source-specific molecular markers such as a levoglucosan isomer (primary biomass burning tracer), nitrophenolic compounds (3-methyl-4-nitrocatechol, nitroguaiacol) formed by oxidation of aromatic precursors, and biogenic oxidation products (pinic acid, norpinonic acid, MBTCA) of α-pinene. Volatility distribution analysis identified compounds distributed across the SVOC, LVOC, and ELVOC ranges ($C^* < 300\ \mu g\ m^{-3}$), indicating a significant contribution of functionalized and atmospherically aged compounds. The presence of higher molecular weight compounds (up to m/z 220) suggested potential oligomerization mechanisms responsible for the low-volatility fraction (Kalberer et al., 2004). The highly oxidized product 5-nitrosalicylic acid (O : C ratio = 0.71) indicates ELVOC formation under stable conditions, thus demonstrating the ability of this platform to mimic complex atmospheric aging processes relevant for exposure characterization. These stable, controlled conditions allow for characterization of the aging process from highly volatile precursor molecules to low-volatility products. This process is practically impossible to trace in the ambient atmosphere due to mixed source contributions and oxidation levels.

In both scenarios, SOA formation was the product of VOC oxidation and in the enhanced scenario, primary biomass burning emissions and their atmospheric processing had additional contributions. This dual formation pathway explains the enhanced organic mass fractions and distinct volatility distributions observed between scenarios. These oxidation processes demonstrate the capacity of the platform to reproduce specific atmospheric transformations under controlled conditions. The detection of both ring-retaining and ring-opening products confirms the existence of multiple simultaneous oxidation mechanisms, providing molecular-level validation of urban atmospheric chemistry models.

These volatility distributions provide critical data for atmospheric model parameterization. Current secondary organic aerosol formation models are dependent on limited field observations wherein several sources interact continuously, hence isolating individual transformation processes becomes difficult. The molecular speciation and volatility distributions determined under controlled conditions allow a systematic evaluation of atmospheric chemistry models and an improvement of mechanistic representations. Thus, source-specific transformation pathways known to be difficult to isolate in ambient measurements become available for evaluation through the use of atmospheric simulation chambers. This leads to stronger predictive capacities of regional air quality models.

Detection of primary emission markers (levoglucosan), and secondary products (pinic acid, norpinonic acid, MBTCA) (Christoffersen et al., 1998; Jang, 1999; Mutzel et

al., 2016; Yang et al., 2016), confirms the ability of the platform to reproduce direct emissions as well as atmospheric transformations (Ho et al., 2007; Kawamura and Kaplan, 1987; Yang et al., 2016). Nitrophenolic compounds, identified as abundant species in biomass burning aerosols (Lin et al., 2016), are specific molecular markers for residential heating emissions. They have not only been detected in biomass burning aerosols from biogenic sources but also in suburban and urban regions during wintertime, because of the widespread domestic wood burning for heating. Detection of methyl-nitrocatechols and methyl-nitrophenols, as products of m-cresol photooxidation from wood combustion, provides molecular-level tracers for source apportionment in exposure studies. Several compounds that originated from biogenic and anthropogenic precursor oxidation were detected in both scenarios, although more comprehensive detections were achieved with the biomass burning enhanced conditions due to higher concentrations of organic aerosol. We identified compounds in both scenarios including 4,6-dinitro-o-cresol (a product of aromatic precursor oxidation under high NO_x), dimethyl-nitrophenol (a product of m-xylene oxidation), and cis-pinonic acid (a product of α-pinene ozonolysis and OH radical oxidation).

Hildebrandt Ruiz et al. (2015) emphasized the influence of photochemical aging on organic aerosols, highlighting the progressive oxidation of organic compounds which resulted in highly oxidized low-volatility aerosol species. Paciga et al. (2016) evaluated the dominance of organic nitrogen compounds in secondary organic aerosols, providing additional insights into the distribution of semi-volatile, low-volatility, and extremely low-volatility organic aerosol compounds. The pyrolysis of lignin during biomass burning produces substituted phenols (i.e., alkylphenols, methoxyphenols), which undergo further oxidations with atmospheric radicals, primarily hydroxyl radicals (OH), or through NO_2 addition reactions, leading to the formation of nitrophenols (Haque et al., 2019; Simoneit et al., 1999; Yang et al., 2016). Beyond their utility as source tracers, these compounds have pro-oxidant and cytotoxic properties demonstrated in previous laboratory studies (Keith and Telliard, 1979; Khan et al., 2022). This detailed chemical characterization facilitates mechanistic studies linking specific molecular components to biological responses under reproducible exposure conditions.

4.3 Wall effects and experimental stability

Wall effects are an inherent consideration in extended chamber experiments. Particle wall losses have not been specifically investigated during these experiments but were characterized in previous work: polydisperse ammonium sulfate particles (submicronic) and dusts (supermicronic) were injected into CESAM, and the number size distribution was measured as a function of time to derive first-order decay rates for each size bin. These experimental loss rates were well reproduced using the parametrization of Lai and Nazaroff (2000). The aerosol lifetime in CESAM was determined to range from 10 h to 4 d depending on particle size distribution, which is therefore quite long, although not negligible for experiments lasting several days as in this study. These losses would need to be considered when performing numerical simulations, which was not the case here.

The loss of semi-volatile species has also been investigated in previous studies and found to be highly dependent on the wall state (Suarez-Bertoa et al., 2012). A passivation of the walls was observed when repeating the same experiment over several days, leading to a decreasing wall loss rate for the semi-volatile compounds injected. The impact of heterogeneous reactions occurring on the walls on gas-phase composition has also been investigated in CESAM; for example, the reduction of NO_2 into HONO has been observed, and identified heterogeneous wall reactions are described in an "auxiliary mechanism" (Wang et al., 2011).

Taken together, these considerations confirm that particles and semi-volatile compounds may be lost on the walls, affecting the composition of the mixture. However, this study does not aim to investigate detailed chemical processes but to generate mixtures representative of urban atmospheres. What matters here is the composition of the mixture actually reaching the exposure isolator. Considering that experiments last for several days, we expect that chamber walls progressively passivate, leading to an equilibrium between emissions, losses, and partitioning between gas-particles and walls. This is supported by the stability of the dilution ratio between CESAM and the exposure isolator throughout both experimental periods, consistent with the nominal 1 : 10 design specification, as well as by the day-by-day stability of the aerosol size distribution (Fig. S1a–b, Supplement). Such heterogeneous wall reactions have not been observed to lead to new compounds affecting SOA composition.

Concerning the photolysis of products, considering that the actinic flux in CESAM closely approximates the solar spectrum, photochemistry is expected to be representative of that occurring in the real atmosphere (Wang et al., 2011).

Some aspects of the platform present additional limitations. Ozone concentrations remained low due to rapid NO-O_3 reactions and chamber surface interactions. The molecular characterization was based on offline filter analysis rather than time-resolved measurements of transformation products. The targeted molecular markers were not quantified comprehensively in the exposure isolator. In addition, the experiment did not determine an integrated OH exposure or an equivalent atmospheric age, and it did not resolve transient intermediates or radical chemistry products.

Irradiation was maintained continuously throughout the 7 d experiments without day/night cycling. While this ensures stable aerosol generation for chronic biological exposure, it differs from ambient photochemical cycle between OH-dominated daytime and NO_3-dominated nighttime chemistry. Relative humidity and temperature were held

constant across both scenarios (RH 30 %–50 %, T 22–25 °C) to ensure experimental comparability. Real biomass burning episodes typically occur at higher RH (60 %–80 %) and lower temperatures, which would enhance gas-particle partitioning.

The standard urban scenario included primary ammonium sulphate seed particles but no primary carbonaceous or traffic-emitted particulate matter. Its organic fraction was intended to result mainly from oxidation of the injected VOC mixture, although the primary and secondary organic fractions were not quantified. Preliminary tests using a MiniCast combustion source to introduce primary carbonaceous particles in this scenario raised concerns regarding animal exposure to residual propane. Filtration and source characterization are therefore technical priorities for future campaigns. In the biomass burning enhanced scenario, the dual primary/secondary origin of organic aerosol was assessed through molecular markers rather than formal source apportionment. Positive matrix factorization (PMF) analysis of the ACSM organic mass spectra was not performed in this study. Finally, polycyclic aromatic hydrocarbons (PAHs), a recognized class of biomass burning emission products, could not be characterized with the current UPLC/ESI-IMS-QTOFMS setup, as electrospray ionization is poorly suited to these non-polar compounds. As noted in Sect. 3.2, comprehensive isolator-level quantification of the targeted SOA markers was not achieved in this campaign. This prevented a systematic comparison of quantified marker concentrations against ambient measurements, which would otherwise strengthen the assessment of atmospheric representativeness at the molecular level. Increasing the number of filters collected per scenario, or using more sensitive pre-concentration and quantification methods, would enable this comparison in future campaigns.

4.4 Perspectives

Nonetheless, promising developments can be achieved in the future. Ozone generation thus represents a priority to better reflect urban photochemical conditions. Extending the exposure durations while maintaining atmospheric stability presents technical challenges which will require systematic investigation. Mechanistic understanding would be enhanced through the integration of advanced analytical techniques. Chemical ionization mass spectrometry (CIMS) would allow real-time detection of highly reactive species, while derivatization methods would better capture reactive intermediates. Platform expansion should involve a variety of scenarios, from low-polluted to high-polluted urban environments, enabling standardized exposure assessments across pollution levels. The inclusion of additional source-specific scenarios (e.g., industrial, agricultural, marine) would help ensure full exposure characterization across different urban settings. Finally, the integration of real-time molecular analyses would offer a complementary temporal resolution for the transformation processes, linking controlled mechanistic laboratory studies with field observations.

Direct OH measurement in CESAM, while outside the scope of this study, represents a valuable future direction that could enable finer comparison between the simulated and ambient atmospheres. Recent developments in nitrate-ion CIMS instrumentation (Alage et al., 2024) represent a promising potential option for future integration of real-time monitoring with this platform. Gas chromatography-mass spectrometry (GC-MS) would complement the current approach for the characterization of PAHs. Elemental and metal characterization by ICP-MS or real-time instrumentation (an Xact instrument has since been used in more recent PolluRisk campaigns) would provide additional insight into the oxidative potential of biomass burning aerosols. Formal PMF analysis of ACSM organic mass spectra would allow quantitative apportionment of primary and secondary organic aerosol fractions.

Future work could also explore exposing mice to variable or cyclic atmospheres to approach more realistic exposure patterns than the stable conditions used in this study.

5 Conclusions

This molecular-level characterization of urban aerosol analogues under controlled conditions offered detailed insights into source-specific chemical signatures. The identification of 32 distinct organic compounds, including nitrophenolic markers from biomass burning and oxidized aromatics from traffic emissions, contributes to understanding secondary organic aerosol formation and gas-particle partitioning in urban environments. This study provides a controlled chemical framework for separate biological exposure experiments.

The PolluRisk platform demonstrates the feasibility of chronic biological exposure to chemically characterised urban atmospheres. Systematic investigation of emission source contributions under controlled atmospheric conditions facilitates the isolation of specific processes, which are otherwise difficult to conduct in complex ambient environments. The capacity of the platform to generate reproducible atmospheric scenarios opens perspectives for toxicological investigations that may examine links between specific molecular components and biological responses. The potential to extend this approach to cities with different levels of pollution will strengthen comparative studies across different urban contexts.

Data availability. All data presented in the study are included in the paper and Supplement. Raw mass spectrometry data (UPLC/ESI-IMS-QTOFMS and PTR-TOF-MS) are available at Zenodo: https://doi.org/10.5281/zenodo.19546628 (Al Marj, 2026). Additional needs can be directed to the corresponding author.

Supplement. The supplement related to this article is available online at https://doi.org/10.5194/acp-26-13645-2026-supplement.

Author contributions. EAM conducted the investigation and filter analysis, wrote the original draft, performed the data analysis and visualization. AD and JCMR reviewed the manuscript. AG provided the expertise on the filter analysis and reviewed the manuscript. MLT contributed to the filter analysis and data analysis. MC, EP, AB, CG, TB, and EM provided technical resources. BPV and JFD participated in the conceptualization and methodology of the study design. CB participated in the investigation. SL and PC are the principal investigators of the study. All authors made contributions to this work and approved the final version of the manuscript.

Competing interests. The contact author has declared that none of the authors has any competing interests.

Disclaimer. Publisher's note: Copernicus Publications remains neutral with regard to jurisdictional claims made in the text, published maps, institutional affiliations, or any other geographical representation in this paper. The authors bear the ultimate responsibility for providing appropriate place names. Views expressed in the text are those of the authors and do not necessarily reflect the views of the publisher.

Acknowledgements. The authors would like to thank the technical teams of LISA, IMRB and OSU-EFLUVE for their support and assistance. The CNRS-INSU is acknowledged for supporting CESAM chamber as a national facility. The authors acknowledge PRAMMICS Platform from OSU-EFLUVE UMS 3563 for the instrument access. This work was supported by the European Union's Horizon 2020 Research and Innovation programme through the EUROCHAMP-2020 Infrastructure Activity and through the REMEDIA project-H2020. The authors also acknowledge the PhD fellowship IDEX program at Université Paris Cité. During the preparation of this work the author(s) used DeepLPro Software (DeepL GmbH, Cologne, Germany) in order to finalize reformulation and language corrections. After using this tool/service, the author(s) reviewed and edited the content as needed and take(s) full responsibility for the content of the published article.

Financial support. This research has been supported by the European Union's Horizon 2020 Research and Innovation programme through the EUROCHAMP-2020 Infrastructure Activity (grant no. 730997) and through the REMEDIA project (grant no. 874753).

Review statement. This paper was edited by Ivan Kourtchev and reviewed by three anonymous referees.

References

AirParif: Emission de polluants atmosphériques et de gaz à effet de serre-Bilan Ile-de-France-Année 2019, https://www.airparif.fr/bilan/2020/bilan-qualite-de-lair-ile-de-france-2019 (last access: 21 September 2026), 2019.

Ait-Helal, W., Borbon, A., Sauvage, S., de Gouw, J. A., Colomb, A., Gros, V., Freutel, F., Crippa, M., Afif, C., Baltensperger, U., Beekmann, M., Doussin, J.-F., Durand-Jolibois, R., Fronval, I., Grand, N., Leonardis, T., Lopez, M., Michoud, V., Miet, K., Perrier, S., Prévôt, A. S. H., Schneider, J., Siour, G., Zapf, P., and Locoge, N.: Volatile and intermediate volatility organic compounds in suburban Paris: variability, origin and importance for SOA formation, Atmos. Chem. Phys., 14, 10439–10464, https://doi.org/10.5194/acp-14-10439-2014, 2014.

Alage, S., Michoud, V., Harb, S., Picquet-Varrault, B., Cirtog, M., Kumar, A., Rissanen, M., and Cantrell, C.: A nitrate ion chemical-ionization atmospheric-pressure-interface time-of-flight mass spectrometer (NO_3^- ToFCIMS) sensitivity study, Atmos. Meas. Tech., 17, 4709–4724, https://doi.org/10.5194/amt-17-4709-2024, 2024.

Al Marj, E.: Mass spectrometry data for molecular-level characterization of urban aerosol analogues in controlled atmospheric simulations, Zenodo [data set], https://doi.org/10.5281/zenodo.19546628, 2026.

Baudic, A., Gros, V., Sauvage, S., Locoge, N., Sanchez, O., Sarda-Estève, R., Kalogridis, C., Petit, J.-E., Bonnaire, N., Baisnée, D., Favez, O., Albinet, A., Sciare, J., and Bonsang, B.: Seasonal variability and source apportionment of volatile organic compounds (VOCs) in the Paris megacity (France), Atmos. Chem. Phys., 16, 11961–11989, https://doi.org/10.5194/acp-16-11961-2016, 2016.

Belgacemi, R., Ribeiro Baptista, B., Justeau, G., Toigo, M., Frauenpreis, A., Yilmaz, R., Der Vartanian, A., Cazaunau, M., Pangui, E., Bergé, A., Gratien, A., Macias Rodriguez, J. C., Bellusci, S., Derumeaux, G., Boczkowski, J., Al Alam, D., Coll, P., Lanone, S., and Boyer, L.: Complex urban atmosphere alters alveolar stem cells niche properties and drives lung fibrosis, Am. J. Physiol. Lung. Cell. Mol. Physiol., 325, L447–L459, https://doi.org/10.1152/ajplung.00061.2023, 2023.

Blayac, M., Yegen, C.-H., Al Marj, E., Rodriguez, J. C. M., Cazaunau, M., Bergé, A., Epaud, R., Coll, P., and Lanone, S.: Acute exposure to realistic simulated urban atmospheres exacerbates pulmonary phenotype in cystic fibrosis-like mice, J. Hazard. Mater., 465, 133340, https://doi.org/10.1016/j.jhazmat.2023.133340, 2024.

Bressi, M., Sciare, J., Ghersi, V., Bonnaire, N., Nicolas, J. B., Petit, J.-E., Moukhtar, S., Rosso, A., Mihalopoulos, N., and Féron, A.: A one-year comprehensive chemical characterisation of fine aerosol ($PM_{2.5}$) at urban, suburban and rural background sites in the region of Paris (France), Atmos. Chem. Phys., 13, 7825–7844, https://doi.org/10.5194/acp-13-7825-2013, 2013.

Christoffersen, T. S., Hjorth, J., Horie, O., Jensen, N. R., Kotzias, D., Molander, L. L., Neeb, P., Ruppert, L., Winterhalter, R., Virkkula, A., Wirtz, K., and Larsen, B. R.: Cispinic acid, a possible precursor for organic aerosol formation from ozonolysis of α-pinene, Atmos. Environ., 32, 1657–1661, https://doi.org/10.1016/S1352-2310(97)00448-2, 1998.

Coll, P., Cazaunau, M., Boczkowski, J., Zysman, M., Doussin, J.-F., Gratien, A., Derumeaux, G., Pini, M., Di Biagio, C., Pangui, E., Gaimoz, C., Hüe, S., Relaix, F., Der Vatanian, A., Coll, I., Michoud, V., Formenti, P., Forêt, G., Thavaratnasingam, L., Amar, A., Lacavalerie, M., Mäder, M., and Lanone, S.:

Pollurisk: an innovative experimental platform to investigate health impacts of air quality, Naples, Italy, WIT Transactions on Ecology and the Environment, WIT Press, Vol. 230, 557–565, https://doi.org/10.2495/AIR180521, 2018.

Crippa, M., El Haddad, I., Slowik, J. G., DeCarlo, P. F., Mohr, C., Heringa, M. F., Chirico, R., Marchand, N., Sciare, J., Baltensperger, U., and Prévôt, A. S. H.: Identification of marine and continental aerosol sources in Paris using high resolution aerosol mass spectrometry, J. Geophys. Res.-Atmos., 118, 1950–1963, https://doi.org/10.1002/jgrd.50151, 2013.

De Gouw, J. and Warneke, C.: Measurements of volatile organic compounds in the earth's atmosphere using proton-transfer-reaction mass spectrometry, Mass Spectrom. Rev., 26, 223–257, https://doi.org/10.1002/mas.20119, 2007.

Donahue, N. M., Robinson, A. L., Stanier, C. O., and Pandis, S. N.: Coupled Partitioning, Dilution, and Chemical Aging of Semivolatile Organics, Environ. Sci. Technol., 40, 2635–2643, https://doi.org/10.1021/es052297c, 2006.

Donahue, N. M., Epstein, S. A., Pandis, S. N., and Robinson, A. L.: A two-dimensional volatility basis set: 1. organic-aerosol mixing thermodynamics, Atmos. Chem. Phys., 11, 3303–3318, https://doi.org/10.5194/acp-11-3303-2011, 2011.

Doussin, J.-F., Fuchs, H., Kiendler-Scharr, A., Seakins, P., and Wenger, J. (Eds.): A practical guide to atmospheric simulation chambers, Springer International Publishing, Cham, https://doi.org/10.1007/978-3-031-22277-1, 2023.

Finlayson-Pitts, B. J. and Pitts, Jr., J. N.: Chemistry of the upper and lower atmosphere, Elsevier, https://doi.org/10.1016/B978-0-12-257060-5.X5000-X, 2000.

Gaimoz, C., Sauvage, S., Gros, V., Herrmann, F., Williams, J., Locoge, N., Perrussel, O., Bonsang, B., D'Argouges, O., Sarda-Estève, R., and Sciare, J.: Volatile organic compounds sources in Paris in spring 2007 – part II: source apportionment using positive matrix factorisation, Environ. Chem., 8, 91–103, https://doi.org/10.1071/EN10067, 2011.

Georgopoulou, M. P., Macias Rodriguez, J. C., Yegen, C.-H., Kaltsonoudis, C., Cazaunau, M., Vasilakopoulou, C. N., Matrali, A., Seitanidi, K., Aktypis, A., Nenes, A., Buissot, C., Gratien, A., Berge, A., Pangui, E., Al Marj, E., Gerard, L., Varrault, B. P., Lanone, S., Coll, P., and Pandis, S. N.: A coupled atmospheric simulation chamber system for the production of realistic aerosols and preclinical model exposure, Air Qual. Atmos. Health, 17, 2909–2930, https://doi.org/10.1007/s11869-024-01611-5, 2024.

Guilloteau, E., Coll, P., Lu, Z., Djouina, M., Cazaunau, M., Waxin, C., Bergé, A., Caboche, S., Gratien, A., Al Marj, E., Hot, D., Dubuquoy, L., Launay, D., Vignal, C., Lanone, S., and Body-Malapel, M.: Murine in utero exposure to simulated complex urban air pollution disturbs offspring gut maturation and microbiota during intestinal suckling-to-weaning transition in a sex-dependent manner, Part Fibre Toxicol, 19, 41, https://doi.org/10.1186/s12989-022-00481-y, 2022.

Haque, Md. M., Kawamura, K., Deshmukh, D. K., Fang, C., Song, W., Mengying, B., and Zhang, Y.-L.: Characterization of organic aerosols from a Chinese megacity during winter: predominance of fossil fuel combustion, Atmos. Chem. Phys., 19, 5147–5164, https://doi.org/10.5194/acp-19-5147-2019, 2019.

Hildebrandt Ruiz, L., Paciga, A. L., Cerully, K. M., Nenes, A., Donahue, N. M., and Pandis, S. N.: Formation and aging of secondary organic aerosol from toluene: changes in chemical composition, volatility, and hygroscopicity, Atmos. Chem. Phys., 15, 8301–8313, https://doi.org/10.5194/acp-15-8301-2015, 2015.

Ho, K. F., Cao, J. J., Lee, S. C., Kawamura, K., Zhang, R. J., Chow, J. C., and Watson, J. G.: Dicarboxylic acids, ketocarboxylic acids, and dicarbonyls in the urban atmosphere of China, J. Geophys. Res., 112, 2006JD008011, https://doi.org/10.1029/2006JD008011, 2007.

Jang, M.: Newly characterized products and composition of secondary aerosols from the reaction of α-pinene with ozone, Atmos. Environ., 33, 459–474, https://doi.org/10.1016/S1352-2310(98)00222-2, 1999.

Jang, M. and Kamens, R. M.: Characterization of secondary aerosol from the photooxidation of toluene in the presence of NO_x and 1-propene, Environ. Sci. Technol., 35, 3626–3639, https://doi.org/10.1021/es010676+, 2001.

Kalberer, M., Paulsen, D., Sax, M., Steinbacher, M., Dommen, J., Prevot, A. S. H., Fisseha, R., Weingartner, E., Frankevich, V., Zenobi, R., and Baltensperger, U.: Identification of Polymers as Major Components of Atmospheric Organic Aerosols, Science, 303, 1659–1662, https://doi.org/10.1126/science.1092185, 2004.

Kawamura, K. and Kaplan, I. R.: Motor exhaust emissions as a primary source for dicarboxylic acids in Los Angeles ambient air, Environ. Sci. Technol., 21, 105–110, https://doi.org/10.1021/es00155a014, 1987.

Keith, L. and Telliard, W.: ES&T Special Report: Priority pollutants: I-a perspective view, Environ. Sci. Technol., 13, 416–423, https://doi.org/10.1021/es60152a601, 1979.

Khan, F., Jaoui, M., Rudziński, K., Kwapiszewska, K., Martinez-Romero, A., Gil-Casanova, D., Lewandowski, M., Kleindienst, T. E., Offenberg, J. H., Krug, J. D., Surratt, J. D., and Szmigielski, R.: Cytotoxicity and oxidative stress induced by atmospheric mono-nitrophenols in human lung cells, Environ. Pollut., 301, 119010, https://doi.org/10.1016/j.envpol.2022.119010, 2022.

Krug, J. D., Lewandowski, M., Offenberg, J. H., Turlington, J. M., Lonneman, W. A., Modak, N., Krantz, Q. T., King, C., Gavett, S. H., Gilmour, M. I., DeMarini, D. M., and Kleindienst, T. E.: Photochemical Conversion of Surrogate Emissions for Use in Toxicological Studies: Role of Particulate- and Gas-Phase Products, Environ. Sci. Technol., 52, 3037–3044, https://doi.org/10.1021/acs.est.7b04879, 2018.

Lai, A. C. K. and Nazaroff, W. W.: Modeling Indoor Particle Deposition From Turbulent Flow Onto Smooth Surfaces, J. Aerosol Sci., 31, 463–476, https://doi.org/10.1016/S0021-8502(99)00536-4, 2000.

Languille, B., Gros, V., Petit, J.-E., Honoré, C., Baudic, A., Perrussel, O., Foret, G., Michoud, V., Truong, F., Bonnaire, N., Sarda-Estève, R., Delmotte, M., Feron, A., Maisonneuve, F., Gaimoz, C., Formenti, P., Kotthaus, S., Haeffelin, M., and Favez, O.: Wood burning: a major source of volatile organic compounds during wintertime in the Paris region, Sci. Total Environ., 711, 135055, https://doi.org/10.1016/j.scitotenv.2019.135055, 2020.

Li, K., Li, J., Tong, S., Wang, W., Huang, R.-J., and Ge, M.: Characteristics of wintertime VOCs in suburban and urban Beijing: concentrations, emission ratios, and festival effects, Atmos. Chem. Phys., 19, 8021–8036, https://doi.org/10.5194/acp-19-8021-2019, 2019.

Li, Y., Pöschl, U., and Shiraiwa, M.: Molecular corridors and parameterizations of volatility in the chemical evolution

of organic aerosols, Atmos. Chem. Phys., 16, 3327–3344, https://doi.org/10.5194/acp-16-3327-2016, 2016.

Lin, P., Aiona, P. K., Li, Y., Shiraiwa, M., Laskin, J., Nizkorodov, S. A., and Laskin, A.: Molecular characterization of brown carbon in biomass burning aerosol particles, Environ. Sci. Technol., 50, 11815–11824, https://doi.org/10.1021/acs.est.6b03024, 2016.

Michoud, V., Sciare, J., Sauvage, S., Dusanter, S., Léonardis, T., Gros, V., Kalogridis, C., Zannoni, N., Féron, A., Petit, J.-E., Crenn, V., Baisnée, D., Sarda-Estève, R., Bonnaire, N., Marchand, N., DeWitt, H. L., Pey, J., Colomb, A., Gheusi, F., Szidat, S., Stavroulas, I., Borbon, A., and Locoge, N.: Organic carbon at a remote site of the western Mediterranean Basin: sources and chemistry during the ChArMEx SOP2 field experiment, Atmos. Chem. Phys., 17, 8837–8865, https://doi.org/10.5194/acp-17-8837-2017, 2017.

Middlebrook, A. M., Bahreini, R., Jimenez, J. L., and Canagaratna, M. R.: Evaluation of Composition-Dependent Collection Efficiencies for the Aerodyne Aerosol Mass Spectrometer using Field Data, Aerosol Sci. Tech., 46, 258–271, https://doi.org/10.1080/02786826.2011.620041, 2012.

Montero, L., Vasconcellos, P. C., Souza, S. R., Pires, M. A. F., Sánchez-Ccoyllo, O. R., Andrade, M. F., and Carvalho, L. R. F.: Measurements of atmospheric carboxylic acids and carbonyl compounds in São Paulo City, Brazil, Environ. Sci. Technol., 35, 3071–3081, https://doi.org/10.1021/es001875g, 2001.

Mutzel, A., Rodigast, M., Iinuma, Y., Böge, O., and Herrmann, H.: Monoterpene SOA: contribution of first-generation oxidation products to formation and chemical composition, Atmos. Environ., 130, 136–144, https://doi.org/10.1016/j.atmosenv.2015.10.080, 2016.

Paciga, A., Karnezi, E., Kostenidou, E., Hildebrandt, L., Psichoudaki, M., Engelhart, G. J., Lee, B.-H., Crippa, M., Prévôt, A. S. H., Baltensperger, U., and Pandis, S. N.: Volatility of organic aerosol and its components in the megacity of Paris, Atmos. Chem. Phys., 16, 2013–2023, https://doi.org/10.5194/acp-16-2013-2016, 2016.

Pereira, D. L., Gratien, A., Giorio, C., Mebold, E., Bertin, T., Gaimoz, C., Doussin, J.-F., and Formenti, P.: Two optimized methods for the quantification of anthropogenic and biogenic markers in aerosol samples using liquid chromatography mass spectrometry and gas chromatography mass spectrometry, Atmos. Meas. Tech., 19, 1–19, https://doi.org/10.5194/amt-19-1-2026, 2026.

Petit, J.-E., Favez, O., Sciare, J., Canonaco, F., Croteau, P., Močnik, G., Jayne, J., Worsnop, D., and Leoz-Garziandia, E.: Submicron aerosol source apportionment of wintertime pollution in Paris, France by double positive matrix factorization (PMF2) using an aerosol chemical speciation monitor (ACSM) and a multi-wavelength Aethalometer, Atmos. Chem. Phys., 14, 13773–13787, https://doi.org/10.5194/acp-14-13773-2014, 2014.

Salameh, T., Sauvage, S., Locoge, N., Gauduin, J., Perrussel, O., and Borbon, A.: Spatial and temporal variability of BTEX in Paris megacity – two-wheelers as a major driver, Atmos. Environ. X, 1, 100003, https://doi.org/10.1016/j.aeaoa.2018.100003, 2019.

Salcedo, D., Onasch, T. B., Dzepina, K., Canagaratna, M. R., Zhang, Q., Huffman, J. A., DeCarlo, P. F., Jayne, J. T., Mortimer, P., Worsnop, D. R., Kolb, C. E., Johnson, K. S., Zuberi, B., Marr, L. C., Volkamer, R., Molina, L. T., Molina, M. J., Cardenas, B., Bernabé, R. M., Márquez, C., Gaffney, J. S., Marley, N. A., Laskin, A., Shutthanandan, V., Xie, Y., Brune, W., Lesher, R., Shirley, T., and Jimenez, J. L.: Characterization of ambient aerosols in Mexico City during the MCMA-2003 campaign with Aerosol Mass Spectrometry: results from the CENICA Supersite, Atmos. Chem. Phys., 6, 925–946, https://doi.org/10.5194/acp-6-925-2006, 2006.

Schymanski, E. L., Jeon, J., Gulde, R., Fenner, K., Ruff, M., Singer, H. P., and Hollender, J.: Identifying Small Molecules via High Resolution Mass Spectrometry: Communicating Confidence, Environ. Sci. Technol., 48, 2097–2098, https://doi.org/10.1021/es5002105, 2014.

Seinfeld, J. H. and Pandis, S. N.: Atmospheric chemistry and physics-from air pollution to climate change., 2nd edn., John Wiley & Sons, 1232 pp., ISBN 978-1-118-59136-9, 2012.

Sillman, S.: The relation between ozone, NO_x and hydrocarbons in urban and polluted rural environments, Atmos. Environ., 33, 1821–1845, https://doi.org/10.1016/S1352-2310(98)00345-8, 1999.

Simoneit, B. R. T., Schauer, J. J., Nolte, C. G., Oros, D. R., Elias, V. O., Fraser, M. P., Rogge, W. F., and Cass, G. R.: Levoglucosan, a tracer for cellulose in biomass burning and atmospheric particles, Atmos. Environ., 33, 173–182, https://doi.org/10.1016/S1352-2310(98)00145-9, 1999.

Slovic, A. D. and Ribeiro, H.: Policy instruments surrounding urban air quality: the cases of São Paulo, New York City and Paris, Environ. Sci. Policy, 81, 1–9, https://doi.org/10.1016/j.envsci.2017.12.001, 2018.

Suarez-Bertoa, R., Picquet-Varrault, B., Tamas, W., Pangui, E., and Doussin, J.-F.: Atmospheric Fate of a Series of Carbonyl Nitrates: Photolysis Frequencies and OH-Oxidation Rate Constants, Environ. Sci. Technol., 46, 12502–12509, https://doi.org/10.1021/es302613x, 2012.

von der Weiden-Reinmüller, S.-L., Drewnick, F., Zhang, Q. J., Freutel, F., Beekmann, M., and Borrmann, S.: Megacity emission plume characteristics in summer and winter investigated by mobile aerosol and trace gas measurements: the Paris metropolitan area, Atmos. Chem. Phys., 14, 12931–12950, https://doi.org/10.5194/acp-14-12931-2014, 2014.

Von Schneidemesser, E., Monks, P. S., Allan, J. D., Bruhwiler, L., Forster, P., Fowler, D., Lauer, A., Morgan, W. T., Paasonen, P., Righi, M., Sindelarova, K., and Sutton, M. A.: Chemistry and the linkages between air quality and climate change, Chem. Rev., 115, 3856–3897, https://doi.org/10.1021/acs.chemrev.5b00089, 2015.

Wang, J., Doussin, J. F., Perrier, S., Perraudin, E., Katrib, Y., Pangui, E., and Picquet-Varrault, B.: Design of a new multi-phase experimental simulation chamber for atmospheric photosmog, aerosol and cloud chemistry research, Atmos. Meas. Tech., 4, 2465–2494, https://doi.org/10.5194/amt-4-2465-2011, 2011.

Yang, F., Kawamura, K., Chen, J., Ho, K., Lee, S., Gao, Y., Cui, L., Wang, T., and Fu, P.: Anthropogenic and biogenic organic compounds in summertime fine aerosols (PM2.5) in Beijing, China, Atmos. Environ., 124, 166–175, https://doi.org/10.1016/j.atmosenv.2015.08.095, 2016.